Advances in Geo-Energy Research

Vol. 15, No. 1, p. 79-86, 2025

Short communication

Characterization of water micro-distribution behavior in shale nanopores: A comparison between experiment and theoretical model

Xinghe Jiao[1], Wu He[1], Zhenhua Tian[2], Shangwen Zhou[3], Han Wang[1], Yuxuan Xia[1]*

[1]*State Key Laboratory of Petroleum Resources and Engineering, China University of Petroleum, Beijing 102249, P. R. China*
[2]*Research Institute of Exploration and Development, PetroChina Changqing Oilfield Company, Xi'an 710018, P. R. China*
[3]*National Elite Institute of Engineering, CNPC, Beijing 100096, P. R. China*

Keywords:
Adsorbed water
free water
adsorption ratio equation
nuclear magnetic resonance
centrifugation

Cited as:
Jiao, X., He, W., Tian, Z., Zhou, S., Wang, H., Xia, Y. Characterization of water micro-distribution behavior in shale nanopores: A comparison between experiment and theoretical model. Advances in Geo-Energy Research, 2025, 15(1): 79-86.
https://doi.org/10.46690/ager.2025.01.08

Abstract:
Due to the existence of fracturing fluid and formation water in shale gas reservoirs, the coexistence of gas and water in nanopores is prevalent. The pore water in the reservoir, on the one hand, affects gas flow behavior and permeability. On the other hand, it blocks pore throats and occupies adsorption sites on the pore surface, consequently reducing the gas adsorption capacity. The occurrence of pore water in shale reservoirs holds significant importance for shale gas resources exploration and development. In this paper, the shale from the Longmaxi Formation, Sichuan Basin was selected as the research target. The content and micro-distribution behavior of pore water were evaluated through centrifugation-nuclear magnetic resonance experiment and theoretical model. The results demonstrated that the content of free water would be underestimated by the experiment, with 2.55%-6.80% lower than that calculated by theoretical model. Moreover, due to the limitations of nuclear magnetic resonance experiment, the adsorbed water in mesopores and macropores might be mistakenly identified as that in smaller pores. As a result, the theoretical model is more applicable for characterizing the micro-distribution behavior of pore water than the origin nuclear magnetic resonance data.

1. Introduction

Shale gas, a unique unconventional resource, holds extensive prospects for exploration and development, which mainly exists in the nanopores with free, adsorbed, and dissolved state (Yu et al., 2021). In contrast to conventional reservoirs, shale reservoirs display the low porosity and extremely low permeability. Horizontal drilling and hydraulic fracturing are the crucial methods for the exploitation of shale gas reservoirs (Estrada and Bhamidimarri, 2016; Wu et al., 2025). However, after hydraulic fracturing, only a small amount of fracturing fluid returns to the wellbore (approximately 25% to 60%), and most of them remains retained within the reservoir (Li et al., 2019). Consequently, the coexistence of gas and water is a ubiquitous characteristic in shale gas reservoirs. Among them, pore water in shale nanopores mainly exhibits adsorbed and free state (Fan et al., 2023). Adsorbed water primarily adsorbs on the surfaces of clay minerals and oxygen-containing functional groups of organic matter, and remains usually immobile under the action of external forces, while free water is mainly stored in the center of pores, with high mobility and a tendency to flow under external influence (Boampong et al., 2022; Zhang et al., 2022).

Shale pores are mostly at the nanometer scale and exhibit pronounced scale and surface effects, the structure and occur-

*Corresponding author.
E-mail address: jiaoxinh1@163.com (X. Jiao); wuhe202208@163.com (W. He); tzhua_cq@petrochina.com.cn (Z. Tian); zhousw10@petrochina.com.cn (S. Zhou); hanwang@cup.edu.cn (H. Wang); xiayx@cup.edu.cn (Y. Xia).

Received October 26, 2024; revised November 21, 2024; accepted December 8, 2024; available online December 13, 2024.

Yandy Scientific Press

Table 1. Basic information of shale samples.

No.	Porosity (%)	Permeability (10^{-3} mD)	Mineral composition (%)						TOC (%)
			Clay	Quartz	Feldspars	Calcite	Dolomite	Pyrite	
S5	3.69	5.72	42.5	49.3	8.2	/	/	/	0.23
S7	3.67	3.91	41.0	49.4	9.6	/	/	/	0.69
S11	3.84	7.82	35.6	42.3	9.6	/	6.0	6.5	0.54
S16	3.63	3.85	35.8	44.8	7.1	4.3	8.0	/	0.55
S26	5.91	10.20	31.5	32.8	7.5	6.9	16.0	5.3	2.42
S31	5.67	7.59	34.0	39.4	7.1	3.8	8.0	7.7	2.26

rence characteristics of adsorbed water deviate substantially from free water (Cai et al., 2024). Molecular simulations are capable of effectively capturing the interaction forces between fluids and pore surfaces, thereby revealing the microscopic occurrence of pore water, and are widely utilized in the investigation of the microscopic features of water at different states in nanopores (Lyu et al., 2023; Zhou et al., 2023; Zhang et al., 2024a). The occurrence behavior of water primarily depends on the wettability of the pore surface (Zhang et al., 2023; Qin et al., 2024) as well as the water content (Xu et al., 2022; Zhang et al., 2024b). In addition, the water vapor isothermal adsorption experiment is also commonly used to investigate the adsorption behavior of water on the shale pore surface, which advantage is studying the occurrence behavior and adsorption content of water at different relative humidity (Bai et al., 2020; Duan et al., 2023; Xie et al., 2023). The adsorption capacity of the surfaces in different shale components for water vapor differ, among which organic matter and clay minerals are generally regarded to have a more substantial impact on water vapor adsorption (Gao et al., 2022; Medeiros et al., 2022). The pore micro-structure also affects the water vapor adsorption behavior, with higher specific surface area (SSA) and porosity leading to a much greater water vapor adsorption amount (Yang et al., 2020). However, in actual shale reservoirs, pore water is mostly in the liquid state, and the water vapor isothermal adsorption is hard to accurately characterize the occurrence behavior of liquid water.

Nuclear magnetic resonance (NMR), as a rapid, non-destructive and convenient method, is often used to characterize the hydrogen-containing fluid properties of unconventional reservoirs (Yuan et al., 2023). The centrifugation method employs the centrifugal force produced by high-speed rotation of the centrifuge as a driving force to overcome the resistance (i.e., capillary pressure) experienced by the fluid. The higher the rotational speed, the greater the centrifugal pressure difference between the two-phase fluids (also be regarded centrifugal force), and water can be drained from smaller pores. It has been found that the combination of high-speed centrifugation and NMR experiment was widely used to quantitatively characterize the content and microscopic distribution behavior of adsorbed and free water (Liu et al., 2018; Meng et al., 2023; Jia et al., 2024). Theoretically, when the centrifugal force is large enough, it can enable all capillary bound water to be transformed into movable water and drained. However, during the actual centrifugation process, the centrifugal force cannot reach infinity, thus underestimating the actual free water content (Testamanti and Rezaee, 2017; Zheng et al., 2023). As a result, based on the relationship between centrifugal force and the content of movable water, Li et al. (2024) established the quantitative characterization method for shale pore water based on centrifugation-NMR data and the adsorption ratio equation for characterizing the behavior of adsorbed water. However, the differences between centrifugation-NMR experiment and theoretical model are rarely compared.

Therefore, in this paper, the content and micro-distribution behavior of pore water (including adsorbed and free water) in shale nanopores were analyzed based on centrifugation-NMR experiment and theoretical model, respectively, and the differences between them were discussed. Moreover, the thickness of adsorption layer and the density of the adsorbed water were calculated through adsorption ratio equation.

2. Materials and methodology

2.1 Materials

The samples were from Well DA101 in the Da'an area, Sichuan Basin, with the burial depth of exceeding 3,500 m. Samples are all in cylindrical shape, with the diameter of 25 mm and the length of 50 mm. The porosity of the samples was calculated by Boyle's law, the permeability of the samples was measured by pulse decay method, the mineral composition was measured by X-ray diffraction, and the total organic carbon (TOC) content was measured by carbon-sulfur analyzer. The basic information of the samples is presented in Table 1.

2.2 LTNA experiment

Low-temperature nitrogen adsorption (LTNA) experiment was conducted at 77.3 K to obtain the nitrogen adsorption-desorption curves. The adsorption-desorption curves of the samples are of type IV(a), and the type of hysteresis loop is H3, suggesting that slit pores are mainly developed with relatively good connectivity. The Barrett-Joyner-Halenda method was employed to calculate the average pore diameter (APD)

Table 2. Pore structure parameters of shale samples.

No.	N_{2max} (cm^3/g)	SSA (m^2/g)	PV (mm^3/g)	APD (nm)
S5	10.876	4.481	16.823	14.285
S7	12.083	4.544	18.849	15.523
S11	12.741	3.362	12.951	14.519
S16	10.820	4.949	16.916	12.561
S26	14.555	8.513	22.511	10.325
S31	16.512	8.726	25.934	11.326

and pore volume (PV) (Barrett et al., 1951). The Brunauer-Emmet-Teller model was utilized to calculate the SSA (Brunauer et al., 1938). The N_{2max}, SSA, PV, and APD of the shale samples by LTNA are presented in Table 2.

2.3 Centrifugation-NMR experiment

The experiment consists of seven steps: (1) Plunger sample were obtained from the shale reservoir; (2) Samples were dried at 70 °C for over 48 h, and an electronic balance measured the sample mass at different times until there was no significant variation; (3) The mass and transverse relaxation time (T_2) spectrum of the dried sample were measured; (4) Place the dried samples into the saturated water unit, and vacuum for about 12 h, after which the saturation pressure is gradually increased to 25 MPa and then saturated for 48 h; (5) Measure the mass and T_2 spectrum of the saturated samples; (6) The saturated samples were protected with soft paper towels and placed in centrifuge tubes, and the samples were centrifuged at 2,000, 4,000, 6,000, 8,000, and 10,000 rpm, respectively, with each rotational speed lasting for 2 h; (7) The mass and T_2 spectrum of the samples were measured separately at the different rotational speeds.

2.4 Theoretical model

The correlation between centrifugal force and the content of movable water, which can be written as (Li et al., 2024):

$$Q_m = \frac{Q_f \Delta p}{\Delta p + \Delta p_L} \tag{1}$$

where Q_m is the movable water content, mg/g; Q_f is the free water content, mg/g; Δp is the centrifugal force, MPa; Δp_L is the median centrifugal force, that is, the centrifugal force corresponding to the situation when the content of movable water reaches half of the maximum content of movable water, MPa.

To quantitatively characterize the thickness and density of the adsorbed water, Li et al. (2023) proposed a adsorption ratio equation, which can be expressed as:

$$r_a = \frac{Q_a}{Q_a + Q_f} = \frac{1}{1 + \frac{\rho_f}{\rho_a}\left(\frac{V_w}{S_w H} - 1\right)} \tag{2}$$

where r_a is the proportion of adsorbed water to the total pore water, %; Q_a is the adsorbed water content, mg/g; V_w is the PV of water-bearing pores, 10^{-3} cm^3/g; S_w is the SSA of water-bearing pores, m^2/g; H is the average thickness of the adsorption layer, nm; ρ_a is the density of adsorbed water, g/cm^3; ρ_f is the density of free water, g/cm^3.

Introducing a dimensionless correction coefficient τ, the relationship between V_w/S_w and Q_f/Q_a is established:

$$\frac{V_w}{S_w} = \tau H \frac{\rho_a}{\rho_f}\frac{Q_f}{Q_a} + \tau H \tag{3}$$

For slit pores, the τ = 1; for non-slit pores, $\tau \neq 1$. The adsorption layer thickness and density of the adsorbed water can be determined from the intercept and slope of the fitted curve.

Based on NMR experiment, the T_2 can be approximately expressed as:

$$\frac{1}{T_2} = \rho_2 \frac{S_w}{V_w} \tag{4}$$

where ρ_2 is the surface relaxation rate, nm/ms.

By combining Eqs. (2) and (4), the r_a corresponding to each T_2 can be calculated:

$$r_{ai} = \frac{1}{1 + \frac{\rho_f}{\rho_a}\left(\frac{T_{2i}\rho_2}{H} - 1\right)} \tag{5}$$

where r_{ai} is the r_a corresponding to each T_2; T_{2i} is the T_2 at the i-th point, ms.

3. Results and discussion

3.1 T_2 spectrum distribution

NMR T_2 spectrum can clearly characterize the distribution behavior of pore water in saturated samples during the centrifugation process. The results for S11 and S26 are shown in Fig. 1. During the centrifugation process, free water is drained under the effect of centrifugal force, while adsorbed water remains in the pore space. Samples saturated with water mostly display the bimodal distribution, which suggests that the pores are mainly occupied by two distinct categories of pores, specifically the smaller-sized and larger-sized ones. The peak value of the main peak is mainly distributed between 0.01 and 3 ms, and the secondary peak is mainly within the range greater than 5 ms. The signal amplitude of the main peak is significantly larger than that of the secondary peak, indicating that the smaller pores account for most of the pores.

By observing the distribution of the T_2 spectrum at different centrifugal rotational speeds, it is found that as the speed increases, the signal amplitude of both the main peak and the secondary peak decrease. The envelope line on the left side of the main peak remains essentially unchanged, whereas the envelope line on the right side of the main peak shifts to the left as the rotational speed increases. The peak value of the main peak exhibits a tendency to shift in the bottom-left direction, and the amplitude corresponding to the peak diminishes progressively. For samples with different TOC content, certain differences exist in the T_2 spectrum of the secondary peaks during the centrifugation process. Samples with lower TOC content (Fig. 1(a)), the signal amplitude of the secondary peak decreases rapidly and close to disappearing under the effect of centrifugal force, indicating

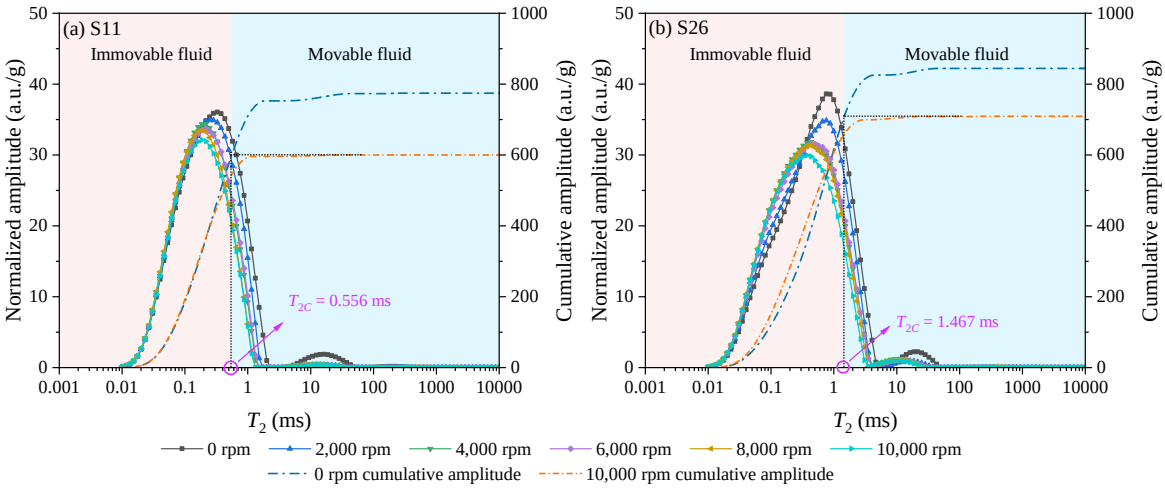

Fig. 1. T_2 spectrum distribution under different centrifugal conditions of (a) S11 and (b) S26.

that the pore water in this portion is largely converted into movable water and discharged. However, for samples with higher TOC content (Fig. 1(b)), the envelope lines on both the left and right sides of the secondary peak shift to the left, and the distribution range of the peak value expands. This indicates that during the centrifugation process, due to the inability to overcome the pore capillary pressure under the centrifugal force, a part of the water fails to be discharged from the pores, resulting in a redistribution of water in the pores (Testamanti and Rezaee, 2017; Jia et al., 2024). In addition, under the centrifugal condition, the signal amplitudes corresponding to the T_2 spectrum of some samples are greater than those corresponding to the saturated water state. This may be attributed to the capillary self-absorption phenomenon in the micropores, which leads to the migration of fluid from large pores to small pores (Zheng et al., 2023).

The T_2 cutoff value (T_{2C}) can reflect the boundary of movable and immovable fluids (Liu et al., 2018; Han et al., 2024). The sample with higher TOC content has the large T_{2C}, as well as more immovable water. This is mainly attributed to the existence of organic matter will lead to alterations in the pore structure, and the oxygen-containing functional groups are in organic matter will adsorb pore water, thereby reducing the diffusion coefficient and modifying the occurrence state. However, in practical situations, the boundary between movable water and immovable water in shale pores is not well-defined. Moreover, studies have already revealed that adsorbed water and free water coexist in shale pores of certain diameter (Li and Cai, 2023). Consequently, the movable and immovable fluids judged by the T_{2C} do not fully conform to the micro-distribution behavior of pore water in actual situations. In the subsequent sections, the micro-distribution behaviors of water in shale pores of different diameter will be analyzed in detail.

3.2 Content of pore water

Accurate differentiation and quantitative characterization of the water content are of crucial importance for understanding the occurrence and diffusion of gases in shale pores. The content of pore water based on experiment and theoretical model is shown in Table 3. The content of total pore water ranges from 12.5583 to 22.5130 mg/g, and its average is 16.3740 mg/g. Among them, based on the centrifugation-NMR experiment, the content of adsorbed water ranges from 9.2831 to 16.4652 mg/g, while the content of free water ranges from 3.2753 to 6.0478 mg/g. However, based on the theoretical model, the content of adsorbed water varies between 9.1164 and 16.0541 mg/g, while the content of free water spans from 3.4419 to 6.4588 mg/g. The free water content calculated by the theoretical model is 2.55%-6.80% higher than that obtained by centrifugation-NMR experiment. Therefore, the content of free water obtained by centrifugation-NMR experiment is usually underestimated. In addition, the proportion of adsorbed water ranges from 65.43% to 75.59% (mean 70.73%), indicating that adsorbed water occupies the dominant position.

Table 3. Quantitative evaluation result of pore water content (mg/g).

No.	Centrifugation-NMR experiment			Theoretical model	
	Q_t	Q_a	Q_f	Q_a	Q_f
S5	13.2180	9.6920	3.5260	9.5661	3.6519
S7	13.5478	9.7105	3.8373	9.5892	3.9586
S11	14.3558	9.5983	4.7575	9.3936	4.9621
S16	12.5583	9.2831	3.2753	9.1164	3.4419
S26	22.0514	16.0123	6.0391	15.8583	6.1931
S31	22.5130	16.4652	6.0478	16.0541	6.4588

Notes: Q_t is the total content of pore water.

3.3 Occurrence state of pore water

Molecular dynamics studies have shown that water in shale nanopores tends to adsorb on the pore surface in an

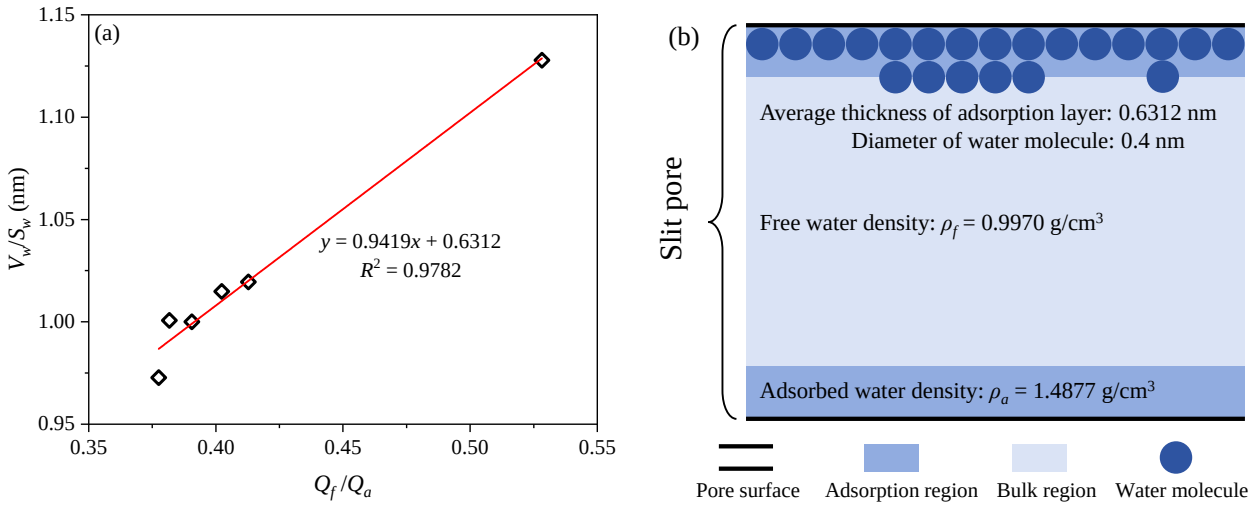

Fig. 2. The relationship between V_w/S_w and Q_f/Q_a (a) and the characteristics of adsorbed water in slit pore (b).

orderly manner, forming one or more adsorption layers (Xu et al., 2020). Based on Eq. (3), the adsorption layer characteristic of the pore water can be determined from the intercept and slope of the fitted curve. This centrifugation-NMR experiment was carried out at the temperature of 25 °C and standard atmospheric pressure, so the density of the water used for saturation (that is free water density) was 0.9970 g/cm^3. As shown in Fig. 2(a), V_w/S_w and Q_f/Q_a exhibit the good positive correlation (R^2 = 0.9782). Based on the LTNA results, the samples are mainly slit pores, so the τ is taken as 1. The average thickness of the adsorption layer is calculated to be 0.6312 nm, and the diameter of the water molecule is approximately 0.4 nm. As a result, a remarkable heterogeneity is manifested in the distribution of adsorbed water within the shale nanopores, with one to two adsorption layers being formed (Fig. 2(b)). Based on the slope and intercept values, the density of the adsorption layer is calculated to be 1.4877 g/cm^3, indicating that the density of the adsorbed water in the nanopores is significantly greater than free water.

3.4 Micro-distribution of pore water

To quantitatively analyze the distribution behavior of adsorbed and free water in nanopores with different pore size, respectively, it is necessary to convert the T_2 spectrum distribution into pore size distribution. Among them, the ρ_2 is the crucial parameter (Saidian and Prasad, 2015). The ρ_2 of samples ranges from 2.111 to 4.435 nm/ms, with an average of 3.460 nm/ms.

There are significant differences in the distribution of adsorbed water and free water obtained through experiment and theoretical model (Fig. 3). Regarding the experimental results, the peak value of the main peak of adsorbed water is greater than that of free water. However, under the calculation results of the theoretical model, the peak value of the main peak of free water is greater than that of adsorbed water. Moreover, based on the distribution of adsorbed water, it can be observed that the adsorbed water in the pores with the diameter between 2 and 10 nm decreases, and the peak value of the main peak of adsorbed water shows a tendency to shift towards the lower left. This indicates that after 10,000 rpm centrifugation, this part of the adsorbed water can still be converted into movable water and drained out. In addition, the range of the main peak of adsorbed water obtained through the theoretical model is larger. The envelope curve on the right side of the main peak shifts to the right compared with the experimental results, indicating that there is still adsorbed water distributed in these pores. This is mainly due to the circumstance that in the centrifugation, certain water within the mesopores and macropores might attach to the pore surfaces, while in the NMR experiment, this attached water is misidentified as being generated by smaller pores (Xia et al., 2024). To sum up, the theoretical model can reflect the distribution of adsorbed water and free water in shale nanopores more accurately.

Micropores basically contain only adsorbed water, while macropores are almost occupied by free water only. However, in mesopores, there is an overlapping part between the adsorbed and the free water signal, indicating that both free and adsorbed water are distributed in these pores. The pore diameter significantly controls the micro-distribution of pore water. There is a distinct separation between the adsorbed water peak and the free water peak, where the adsorbed water peak is located on the right side of the free water peak. This is mainly because adsorbed water is composed of water molecules that are closely attached to the pore surface through hydrogen bonds and van der Waals forces (Liang et al., 2016; Yang et al., 2024). For larger pores, the capillary pressure is lower and the interaction of pore water with the surface is weaker, which is thus unfavorable for the occurrence of adsorbed water. Free water is mainly existence in larger pores, with weaker interaction with the pore surface, so it is easier to be converted into movable water and drained under the effect of centrifugal force. For samples with different TOC contents, the distribution of pore water is also different. As for lower TOC content sample (such as S11), the signal distribution curve of the adsorbed water mainly shows a

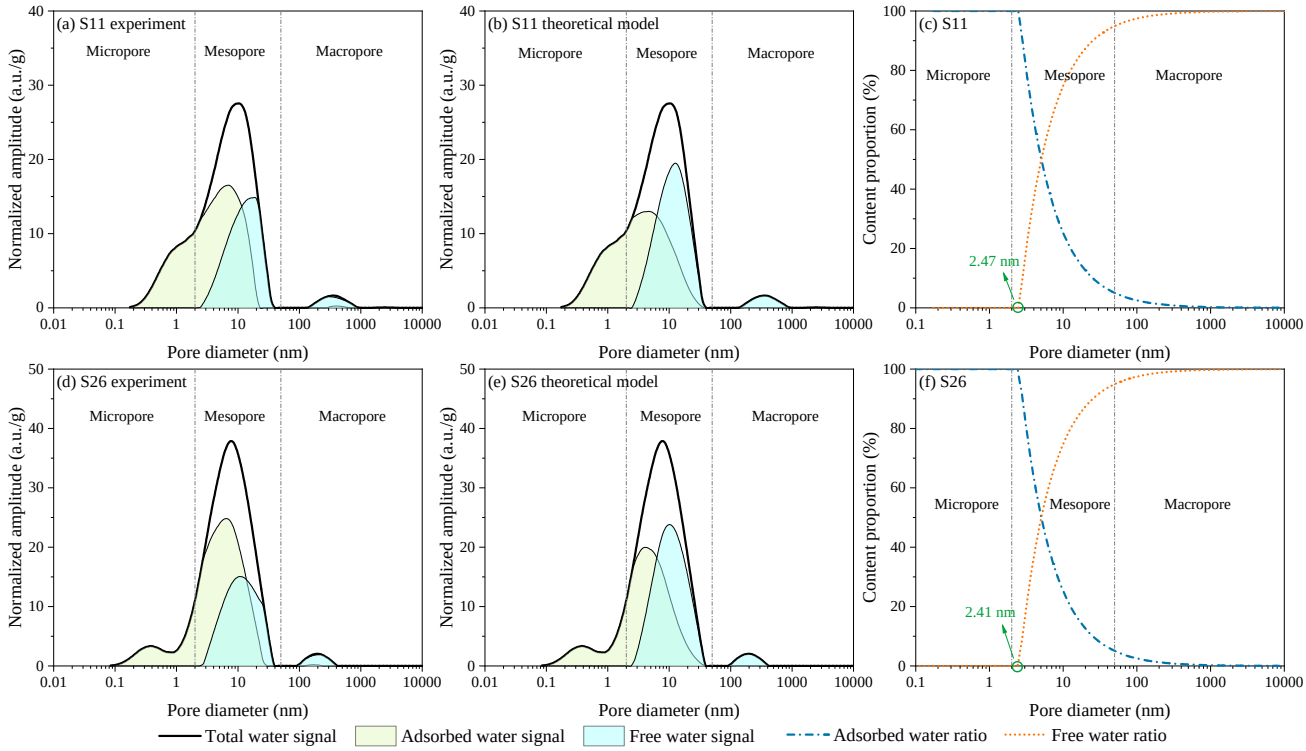

Fig. 3. Adsorbed and free water micro-distribution based on (a) (d) experiment and (b) (e) theoretical model, and (c) (f) content proportion of total water.

unimodal distribution, while the free water and total pore water signal exhibit a multimodal distribution. However, for higher TOC content sample (such as S26), both the adsorbed water and the free water distribution exhibit a bimodal distribution. Among them, the secondary peak of the adsorbed water is distributed in the micropores, while the secondary peak of the free water is distributed in the macropores. A lower limit of pore diameter exists for the distribution of free water (Figs. 3(c) and 3(f)). That is, in pores whose diameter smaller than this lower limit, only adsorbed water exists and there is no free water distribution. The lower limits of S11 and S26 are 2.47 nm and 2.41 nm, respectively, which are greater than the average thickness of the adsorption layer in slit pores calculated above. This is mainly attributed to the fact that in pores with a very small diameter, water molecules are subject to much stronger interactions with the pore surfaces and will form multilayer adsorption (Zhang et al., 2022).

4. Conclusions

In this study, the centrifugation-NMR experiment and theoretical model were employed to analyze the pore water occurrence behavior of six shale samples from the Longmaxi Formation in the Sichuan Basin, and the differences between them were discussed. The main conclusions are as follows:

1) The theoretical model can reflect the content and distribution of pore water (including adsorbed and free water) in shale nanopores more accurately, and can calculate the content of free water more accurately as well as characterize the micro-distribution of adsorbed water in mesopores and macropores.
2) The adsorbed water occupies the dominant position and is predominantly found in micropores and mesopores, while free water is mainly present in mesopores and macropores, with a phenomenon of coexistence of adsorbed and free water in mesopores.
3) The average thickness of the adsorption layer is 0.6312 nm, indicating that the water in the nanopores is mainly forming one to two adsorption layers, and the density of the adsorption layer is 1.4877 g/cm^3.

Acknowledgements

The authors are grateful to the National Natural Science Foundation of China (Nos. 42302143, 52404048).

Conflict of interest

The authors declare no competing interest.

References

Bai, J., Kang, Y., Chen, M., et al. Impact of surface chemistry and pore structure on water vapor adsorption behavior in gas shale. Chemical Engineering Journal, 2020, 402: 126238.

Barrett, E. P., Joyner, L. G., Halenda, P. P. The determination of pore volume and area distributions in porous substances. I. Computations from nitrogen isotherms. Journal of the American Chemical Society, 1951, 73(1): 373-380.

Boampong, L. O., Rafati, R., Sharifi Haddad, A. A calibrated surface complexation model for carbonate-oil-brine interactions coupled with reservoir simulation—Application to controlled salinity water flooding. Journal of Petroleum Science and Engineering, 2022, 208: 109314.

Brunauer, S., Emmett, P. H., Teller, E. Adsorption of gases in multimolecular layers. Journal of the American Chemical Society, 1938, 60(2): 309-319.

Cai, J., Jiao, X., Wang, H., et al. Multiphase fluid-rock interactions and flow behaviors in shale nanopores: A comprehensive review. Earth-Science Reviews, 2024, 257: 104884.

Duan, S., Geng, L., Li, G., et al. Water vapour adsorption isotherms of shales: Thermodynamic properties and microstructure. Fluid Phase Equilibria, 2023, 563: 113583.

Estrada, J. M., Bhamidimarri, R. A review of the issues and treatment options for wastewater from shale gas extraction by hydraulic fracturing. Fuel, 2016, 182: 292-303.

Fan, Q., Cheng, P., Tian, H., et al. Distribution and occurrence of pore water and retained oil in nanopores of marine-terrestrial transitional shales during oil generation and expulsion: Implications from a thermal simulation experiment on shale plug samples. Marine and Petroleum Geology, 2023, 150: 106125.

Fleury, M., Romero-Sarmiento, M. Characterization of shales using T_1-T_2 NMR maps. Journal of Petroleum Science and Engineering, 2016, 137: 55-62.

Gao, Z., Xiong, S., Wei, L. The new multistage water adsorption model of Longmaxi Formation shale considering the spatial configuration relationship between organic matter and clay minerals. Petroleum Science, 2022, 19(5): 1950-1963.

Han, Y., Jiang, Z., Liang, Z., et al. Study on the multifractal characterization and seepage of the shale matrix: A case study of the Longmaxi Formation in southwestern Sichuan Basin, China. Geoenergy Science and Engineering, 2024, 238: 212924.

Jia, T., Zhang, S., Tang, S., et al. Water-bearing properties of high rank coal reservoir and the effect on multiphase methane. Gas Science and Engineering, 2024, 128: 205380.

Liang, L., Luo, D., Liu, X., et al. Experimental study on the wettability and adsorption characteristics of Longmaxi Formation shale in the Sichuan Basin, China. Journal of Natural Gas Science and Engineering, 2016, 33: 1107-1118.

Li, J., Cai, J. Quantitative characterization of fluid occurrence in shale reservoirs. Advances in Geo-Energy Research, 2023, 9(3): 146-151.

Li, J., Wang, Y., Song, Z., et al. Mobility of connate pore water in gas shales: A quantitative evaluation on the Longmaxi shales in the southern Sichuan Basin, China. Marine and Petroleum Geology, 2024, 161: 106674.

Li, J., Zhou, Z., Wang, M., et al. Storage capacity and microdistribution of pore water in gas-producing shales: A collaborative evaluation by centrifugation and nuclear magnetic resonance. Energy & Fuels, 2023, 37(17): 12980-12993.

Li, S., Lei, Q., Wang, X., et al. Permeability regain and aqueous phase migration during hydraulic fracturing shut-ins. Scientific Reports, 2019, 9(1): 1818.

Liu, Y., Yao, Y., Liu, D., et al. Shale pore size classification: An NMR fluid typing method. Marine and Petroleum Geology, 2018, 96: 591-601.

Lyu, F., Ning, Z., Jia, Z., et al. Investigation on gas/water two-phase flow in quartz nanopores from molecular perspectives. Journal of Molecular Liquids, 2023, 371: 121145.

Medeiros, D. C. C. S., Chelme-Ayala, P., Benally, C., et al. Review on carbon-based adsorbents from organic feedstocks for removal of organic contaminants from oil and gas industry process water: Production, adsorption performance and research gaps. Journal of Environmental Management, 2022, 320: 115739.

Meng, M., Ge, H., Shen, Y., et al. Insight into water occurrence and pore size distribution by nuclear magnetic resonance in marine shale reservoirs, southern China. Energy & Fuels, 2023, 37(1): 319-327.

Mu, Y., Hu, Z., Shen, R., et al. Water occurrence characteristics of gas shale based on 2D NMR technology. Energy & Fuels, 2022, 36(2): 910-921.

Qin, X., Wu, J., Xia, Y., et al. Multicomponent image-based modeling of water flow in heterogeneous wet shale nanopores. Energy, 2024, 298: 131367.

Saidian, M., Prasad, M. Effect of mineralogy on nuclear magnetic resonance surface relaxivity: A case study of Middle Bakken and Three Forks Formations. Fuel, 2015, 161: 197-206.

Testamanti, M. N., Rezaee, R. Determination of NMR T_2 cut-off for clay bound water in shales: A case study of Carynginia Formation, Perth Basin, Western Australia. Journal of Petroleum Science and Engineering, 2017, 149: 497-503.

Wei, J., Yang, E., Li, J., et al. Nuclear magnetic resonance study on the evolution of oil water distribution in multi-stage pore networks of shale oil reservoirs. Energy, 2023, 282: 128714.

Wu, M., Chang, X., Guo, Y., et al. Advances, challenges, and opportunities for hydraulic fracturing of deep shale gas reservoirs. Advances in Geo-Energy Research, 2025, 15(1): 1-4.

Xia, X., Xia, Y., Zhao, F., et al. Evaluating the surface relaxivity and movable fluid of low-permeability sandstones based on low-field nuclear magnetic resonance. Physics of Fluids, 2024, 36(11): 116619.

Xie, W., Wang, H., Chen, S., et al. Water adsorption and its pore structure dependence in shale gas reservoirs. Langmuir, 2023, 39(30): 10576-10592.

Xu, H., Yu, H., Fan, J., et al. Two-phase transport characteristic of shale gas and water through hydrophilic and hydrophobic nanopores. Energy & Fuels, 2020, 34(4): 4407-4420.

Xu, J., Zhan, S., Wang, W., et al. Molecular dynamics simulations of two-phase flow of n-alkanes with water in quartz nanopores. Chemical Engineering Journal, 2022, 430: 132800.

Yang, R., Jia, A., He, S., et al. Water adsorption characteristics of organic-rich Wufeng and Longmaxi Shales, Sichuan Basin (China). Journal of Petroleum Science and Engineering, 2020, 193: 107387.

Yang, Y., Song, H., Imani, G., et al. Adsorption behavior of shale oil and water in the kerogen-kaolinite pore by molecular simulations. Journal of Molecular Liquids, 2024, 393: 123549.

Yu, H., Xu, H., Fan, J., et al. Transport of shale gas in microporous/nanoporous media: Molecular to pore-scale simulations. Energy & Fuels, 2021, 35(2): 911-943.

Yuan, Y., Rezaee, R., Zhou, M. -F., et al. A comprehensive review on shale studies with emphasis on nuclear magnetic resonance (NMR) technique. Gas Science and Engineering, 2023, 120: 205163.

Zhang, C., Yao, Y., Swennen, R., et al. Combined effects of the chemical structure and nanopore development on water vapor/liquid adsorption in shale kerogen. Colloids and Surfaces A: Physicochemical and Engineering Aspects, 2022, 653: 129920.

Zhang, D., Tang, H., Song, Y., et al. Molecular simulation of the competitive adsorption of methane and carbon dioxide in the matrix and slit model of shale kerogen and the influence of water. Geoenergy Science and Engineering, 2024a, 242: 213212.

Zhang, L., Yan, W., Fu, J., et al. Methane gas transport in Ca-MMT shale nanoslits considering water content effects: Insights from molecular dynamics simulations. Langmuir, 2024b, 40(47): 25110-25117.

Zhang, S., Wang, T., Gao, Z., et al. Wettability controlling effects on the fluid occurrence and flow in shale gas reservoirs: Present problems and new sights. Capillarity, 2023, 9(2): 25-31.

Zhao, T., Xu, S., Hao, F. Differential adsorption of clay minerals: Implications for organic matter enrichment. Earth-Science Reviews, 2023, 246: 104598.

Zheng, S., Yao, Y., Liu, D., et al. Re-evaluating the accurate multiphase water distribution in coals: Unifying experiment and theory. Chemical Engineering Journal, 2023, 464: 142637.

Zhou, Z., Li, J., Song, Z., et al. Occurrence characteristics of water in nano-slit pores under different solution conditions: A case study on kaolinite. ACS Omega, 2023, 8(21): 18990-19001.